JOURNAL OF GEOPHYSICAL RESEARCH, VOL. 93, NO. C10, PAGES 12,423–12,437, OCTOBER 15, 1988

On the Seasonal Variability of the Alaska Coastal Current

WALTER R. JOHNSON, THOMAS C. ROYER AND JOHN L. LUICK

Institute of Marine Science, University of Alaska Fairbanks

Current measurements of the Alaska Coastal Current were analyzed for their mean structures and seasonal cycles. The current is westward (alongshore) at the surface, 25 to 175 cm s^{-1}, with a baroclinic shear of 30 cm s^{-1} in the upper 70 m. The amplitude of the seasonal variation of the flow decreases with depth, and its maximum phase delay of 3 months occurs at 175 m relative to the surface. The amplitude of the seasonal cycle of the north-south (cross-shore) flow is a minimum at mid-depth. The phase of this seasonal cycle is also delayed at deeper depths, but the maximum shift relative to the surface occurs at 110 m rather than at the bottom (175 m). Empirical orthogonal function analysis indicates that the first mode of the alongshore flow has nearly constant amplitude with depth (barotropic variations) and is related to the east-west wind. The second mode explains significant variance of the surface current and the freshwater discharge. The cross-shore flow analysis shows that the first mode is again nearly barotropic and is principally related to the east-west wind, with increased southward flow when the winds are increased westward. The second mode of the cross-shore flow fluctuates with runoff such that the offshore flow at the surface and the onshore flow near to the bottom coincide with increased freshwater discharge.

INTRODUCTION

Studies of the Alaska Coastal Current in the northern Gulf of Alaska have produced a general description of a current driven by downwelling favorable winds and freshwater discharge [*Royer*, 1979, 1981, 1982; *Schumacher and Reed*, 1980]. The discharge is primarily from a number of small streams, a few large rivers, such as the Copper River, and glacial input. The wind field is dominated (1) in the summer by the North Pacific High, which produces relatively weak winds at the coast, and (2) in the winter by the Aleutian Low, which produces strong westward winds. The seasonal cycle of the current is illustrated by a weak westward flow in June and strong westward flow from September through February. *Royer* [1981] suggested that the maximum in the baroclinic transport occurred in October because of the maximum in discharge.

Early work [*Favorite*, 1974; *Reid and Mantyla*, 1976] treated the circulation in the Gulf of Alaska as a coupled deep ocean-shelf system. The Outer Continental Shelf Environmental Assessment Program (OCSEAP) from 1974 to 1979 resulted in a recognition that the flow was separated into coastal and deep ocean currents. The OCSEAP sampling used horizontal station spacing of 18 km which did not resolve the coastal circulation adequately, though the existence of a coastal current was suggested. Later hydrographic cross sections in the coastal region [*Schumacher and Reed*, 1980; *Royer*, 1981] revealed details of the baroclinic nature of the current. To resolve the temporal variability of this coastal current and evaluate the significance of wind and freshwater forcing, current meter moorings were deployed and eight supporting hydrographic (conductivity-temperature-depth, or CTD) surveys were carried out over 18 months beginning in April 1983.

Paper number 8C0272.
0148-0227/88/008C-0272$05.00

THE DATA

The moored current meter array consisted of two moorings close to each other: one was a surface mooring; the other was a subsurface array. The surface mooring was instrumented from a surface-following buoy with an EG&G vector measuring current meter (VMCM) at 2-m depth and an Aanderaa RCM4 (recording current meter) at 4-m depth (Figure 1). *Johnson and Royer* [1986] presented a detailed description of this surface mooring and the intercomparison of the VMCM and RCM4 data. The subsurface mooring consisted of four Aanderaa RCM4 current meters at 50-, 70-, 110- and 175-m depths. The data recovered are given in Table 1. A hydrographic grid was occupied on the cruises using a Neil Brown Mark III B CTD system (Table 2). A profiling current meter (PCM) was used on the Cape Fairfield section of each cruise. The profiling system consisted of a polyvinyl chloride (PVC) hull and an Aanderaa RCM4 mounted upside down [*Düing and Johnson*, 1972]. Ship drift was estimated by acquiring LORAN C positions over a 20- to 30-min period. No adjustment was made for tidal currents which are approximately 7 to 10 cm s^{-1}. A meteorological station was placed at the coast to provide local wind and precipitation data to supplement the sparse and topographically influenced meteorological data available for this area [*Luick et al.*, 1987]. In addition, winds from the Fleet Numerical Oceanographic Center (FNOC), Monterey, California, were used for comparison with the measured currents.

Hydrographic Results

Cross sections. The hydrographic stations were arranged in sections running approximately perpendicular to the coast (Figure 1). The central line in this study was the Cape Fairfield (CF) line, from the coast (60°30'N) south along 148°W to 58°30'N (stations numbered CF1 through CF15 in Figure 1). Cross sections of salinity on the CF line are used to determine the location of the coastal current. The lowest salinities occur near the coast, and usually a distinct front separates the coastal and shelf water.

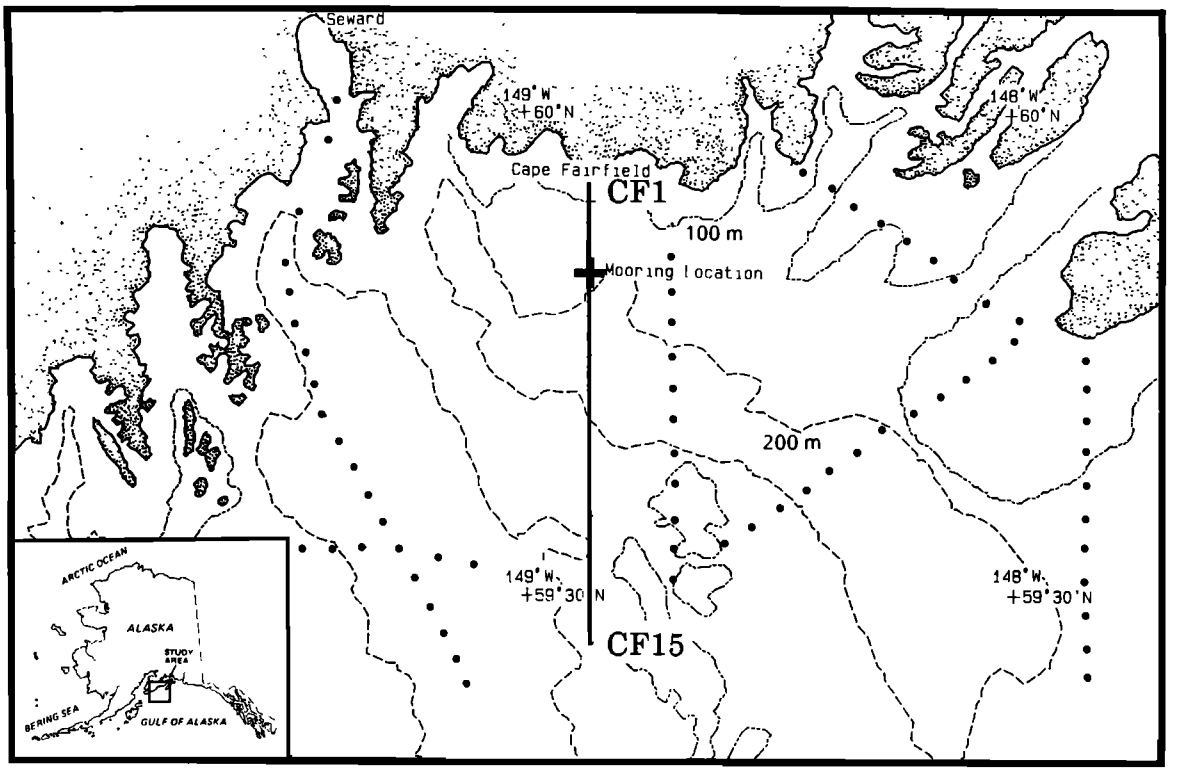

Fig. 1. Chart of the experimental region.

The isohalines slope steeply downward to the north within the coastal current, becoming more level offshore of the jet (Figures 2 and 3).

The seasonal cycle in the hydrographic structure of the coastal current can be described by consideration of the salinity cross section at Cape Fairfield. In late winter (March-April), the near-surface salinity increases from 31.5 parts per thousand (ppt) at the coast to 32.05 ppt 50 km offshore (Figure 2). The steeply rising bottom profile nearshore restricts the width of the surface-to-bottom wind-mixed layer to the inner few kilometers. Offshore of this zone, the vertical salinity gradient is small, varying between 7.5 x 10^{-4} ppt m^{-1} (0.09 ppt/120 m), 4 km offshore, and 1.7 x 10^{-3} ppt m^{-1} (0.25 ppt/150 m) at 50 km. These two gradients imply internal Rossby radii estimates of 2 and 5 km.

In late summer and fall (August-October), at the time of the peak runoff, the near-surface salinities near the coast may decrease to as low as 18.0 ppt (Figure 3). The near-surface salinities at 50 km offshore remain about the same as in spring, 32.5 ± 0.5 ppt. The greatest salinities are at the bottom and often are highest at the midshelf. Of all cruises (Table 2), those in fall recorded both the lowest near-surface and highest near-bottom salinities. The internal Rossby radii change in direct proportion to the vertical salinity gradient, with the springtime estimates increasing to 15 and 30 km, respectively.

At the ranges of temperature, salinity, and pressure involved, density is relatively insensitive to changes in temperature [*Royer*, 1981]. In late winter (March-April), the vertical temperature gradient can be reversed, with the

TABLE 1. Mooring Data Recovery (59°50.4'N, 148°50.0'W)

Instrument	Depth, m	Start Date	End Date
		JA1	
VMCM	2	April, 2 1983	Sept. 8, 1983
RCM4	50	April, 2 1983	Sept. 8, 1983
RCM4	69	April, 2 1983	Sept. 8, 1983
RCM4	111	April, 2 1983	Sept. 8, 1983
RCM4	176	April, 2 1983	Sept. 8, 1983
WLR5	178	April, 2 1983	Sept. 8, 1983
		JA2	
VMCM	2	Sept. 8, 1983	March 31, 1984
RCM4	51	Sept. 8, 1983	March 31, 1984
RCM4	72	Sept. 8, 1983	April 4, 1984
RCM4	113	Sept. 8, 1983	March 30, 1984
RCM4	175	Sept. 8, 1983	March 31, 1984
WLR5	177	Sept. 8, 1983	May 8, 1984
		JA3	
VMCM	2	May 8, 1984	Lost
RCM4	51	May 8, 1984	Oct. 29, 1984
RCM4	70	May 8, 1984	Oct. 29, 1984
RCM4	114	May 8, 1984	Oct. 11, 1984
RCM4	173	May 8, 1984	Oct. 30, 1984
WLR5	175	May 8, 1984	Oct. 30, 1984

TABLE 2. Cruises

Cruise	Start Date	End Date
HX42	April 1, 1983	April 11, 1983
HX45	June 6, 1983	June 12, 1983
HX51	Sept. 7, 1983	Sept. 12, 1983
HX54	Oct. 24, 1983	Oct. 29, 1983
HX55	May 7, 1984	May 12, 1984
HX58	June 4, 1984	June 9, 1984
HX61	Aug. 13, 1984	Aug. 18, 1984
HX65	Oct. 29, 1984	Nov. 3, 1984

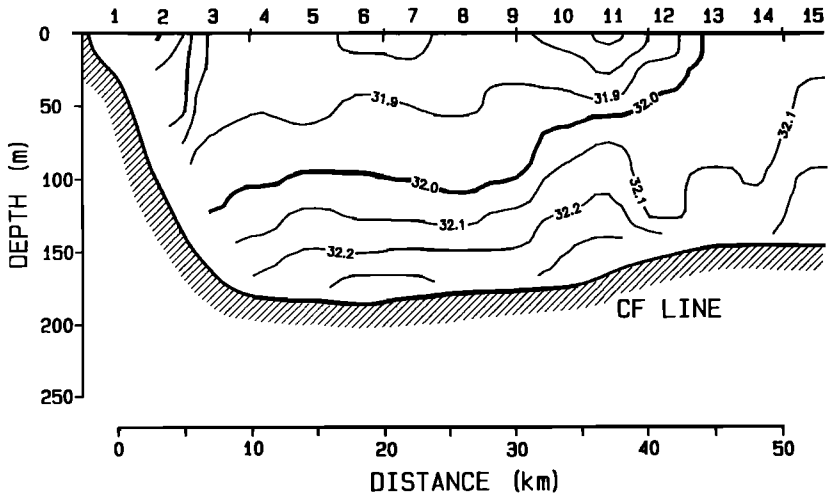

Fig. 2. Cape Fairfield salinity cross section, April 1983.

static stability maintained by the salinity (Figure 4). Typical winter water temperatures range between 3.5° and 6.0°C. Though temperature is not a particularly good tracer of circulation at this time of year, the lowest temperatures tend to be adjacent to the coast as a result of a reduced but continuing cold freshwater inflow.

In summer (July-September), local heating of the low-salinity water produces warm near-surface temperatures, >13°C in a 5- to 10-m-thick layer (Figure 5). The signature of the seasonal warming diffuses downward somewhat faster than salinity [*Xiong and Royer*, 1984]; this will be discussed further below. Since this local heating is nearly uniform horizontally, the surface temperature is nearly uniform, while the salinity preserves its horizontal structure.

Dynamic height distributions. The nearshore dynamic height topography (0/100 dbar) exhibits large seasonal variability (Figure 6), a result of changes in freshwater inflow [*Royer*, 1979]. (The 0/100 dbar dynamic height topography is used as an indicator of the flow as a compromise between a deeper reference level with fewer measurements and a very shallow one that contains more points, but that is not necessarily in geostrophic equilibrium. The 0/100 dbar dynamic height may underestimate the total transport slightly, since the water depths exceeds 100 m. The amount of the underestimation is slightly larger in the winter when the stratification is lowest.) The increases in dynamic height from April 1983 (Figure 6*a*) to September 1983 (Figure 6*c*) are largest near the coast (0.155 dyn m) and are relatively small at the offshore portion of the region (0.025 dyn m). The pattern was reproduced in the 1984 data (Figures 6*e-h*) and is consistent with earlier observations [*Royer*, 1979; *Schumacher and Reed*, 1980]. The horizontal relief of the dynamic height topography reported by *Schumacher and Reed* [1980] was 0.05 to 0.06 in the low-transport season (March-April) and 0.15 to 0.20 in the high-transport season (September-October). The maximum offshore relief observed here was 0.15 dyn m. The two October relief estimates were 0.125 and 0.11 dyn m. The minimum dynamic topography gradient in the data in this study occurred in April 1983 at 0.025 dyn m. The data also

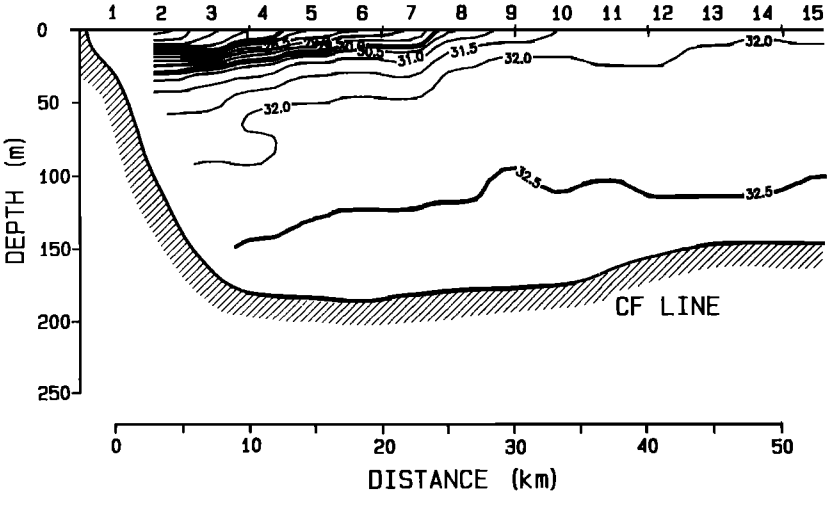

Fig. 3. Cape Fairfield salinity cross section, September 1983.

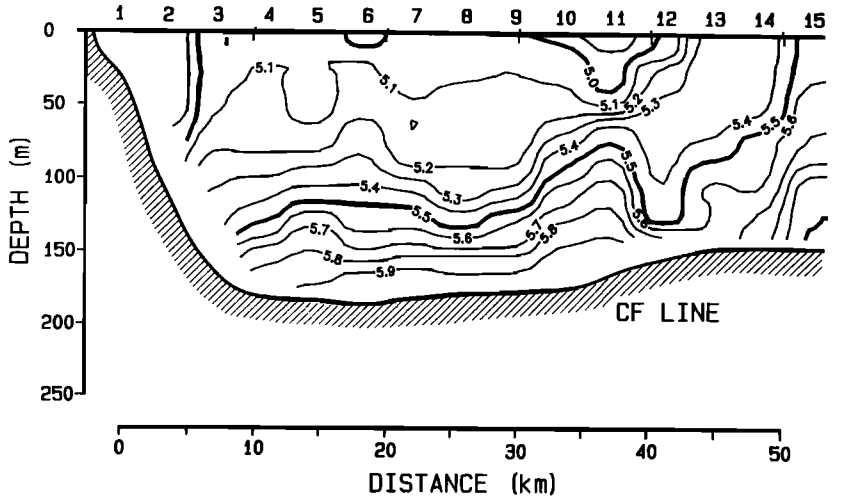

Fig. 4. Cape Fairfield temperature cross section, April 19

support the relationship between sea level at Seward and the dynamic height determined in earlier studies [*Pattullo et al.*, 1955; *Royer*, 1979]. *Royer* [1979] stressed the importance of freshwater discharge to the dynamic height variability.

Although the seasonal changes in dynamic height are greatest at the inner shelf, the curvature of the contours can be large throughout the region. The period of highest dynamic height at the coast was also the period of greatest curvature in the coastal current across the shelf (Figure 6). The largest curvatures, including closed contours in some cases, occurred in August 1984 and September 1983. In September 1983 the contours appeared to follow the bottom topography, suggesting topographic control. Note that the bottom shoals toward the outer portion of the CF and CJ sections. In August 1984, small-scale variations occurred in the dynamic height.

The baroclinic geostrophic transport across the Cape Fairfield line from the coast to CF13 relative to 100 dbar underwent a fourfold seasonal increase in the course of the experiment, with a minimum of 0.08 x 10^6 m^3 s^{-1} in early spring and a maximum of 0.38 x 10^6 m^3 s^{-1} in autumn. The observed mean was 0.21 x 10^6 m^3 s^{-1}. This is in accord with a 10:1 amplification factor for ocean current to freshwater discharge suggested by *Mork* [1981], since the mean runoff is estimated as 23 x 10^3 m^3 s^{-1} [*Royer*, 1982]. While the nearshore dynamic height anomaly decreased between September and October 1983, the transport increased.

Profiling Current Meter (PCM) Cross Sections

The cross sections of eastward velocity component (u, alongshore) provide a complementary description of the seasonal cycle of the current. The PCM cross sections reveal the strength of the current and its offshore position. The April 1983 section of u has a maximum velocity of 80 cm s^{-1} westward (westward will be defined as negative) in the core of the jet (Figure 7*a*). The core was centered about 18 km offshore, between stations CF5 and CF6. The jet was shallow, with the -25 cm s^{-1} contour only 30 m deep at CF6. A flow reversal occurred between CF8 and CF10,

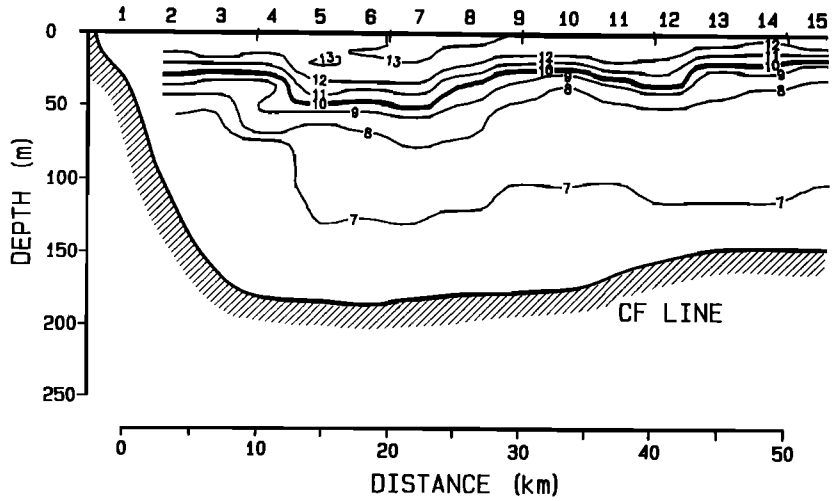

Fig. 5. Cape Fairfield temperature cross section, September 1983.

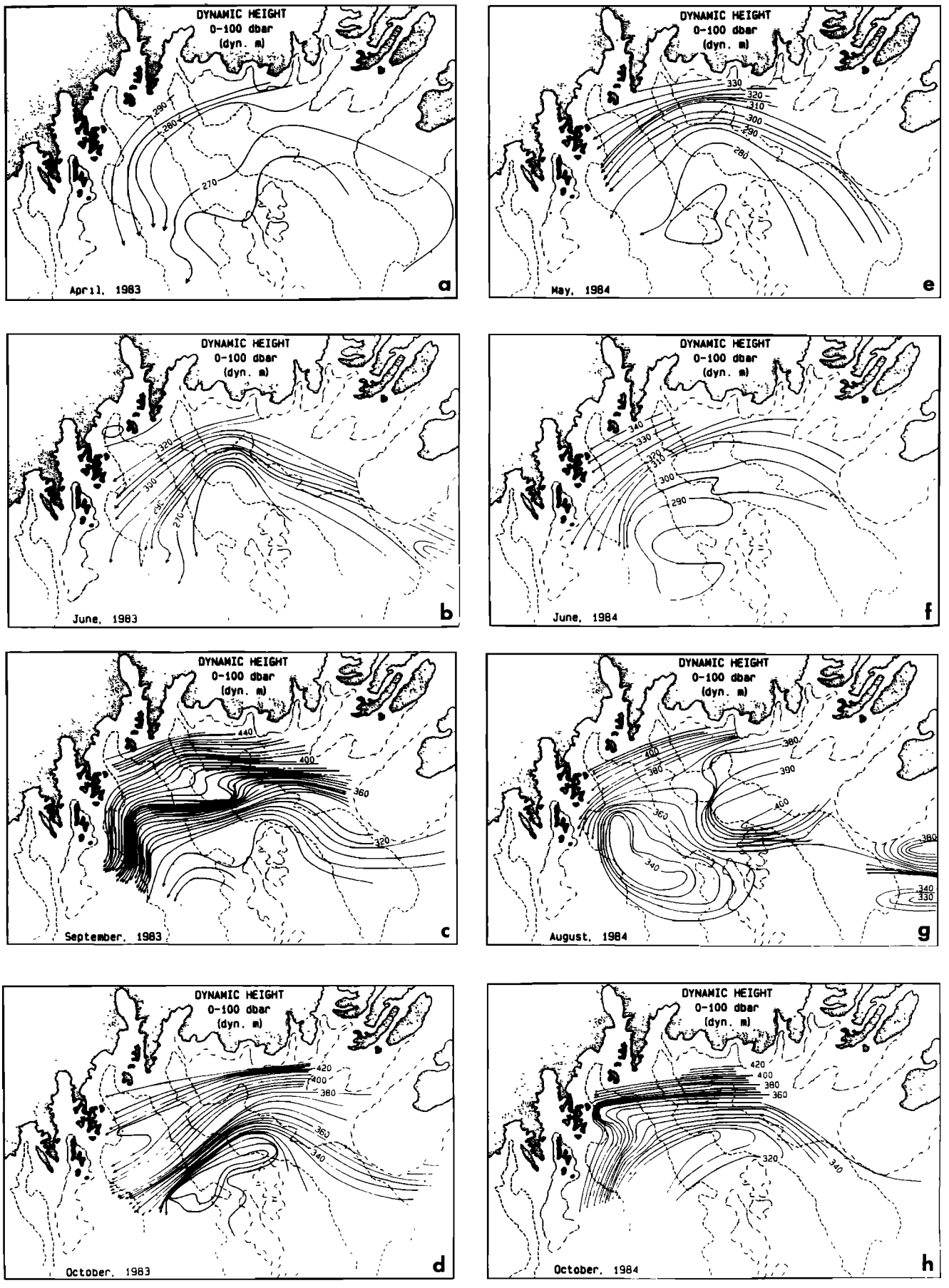

Fig. 6. Dynamic height (geopotential) in dynamic meters for (*a*) April 1983, (*b*) June 1983, (*c*) September 1983, (*d*) October 1983, (*e*) May 1984, (*f*) June 1984, (*g*) August 1984, and (*h*) October 1984.

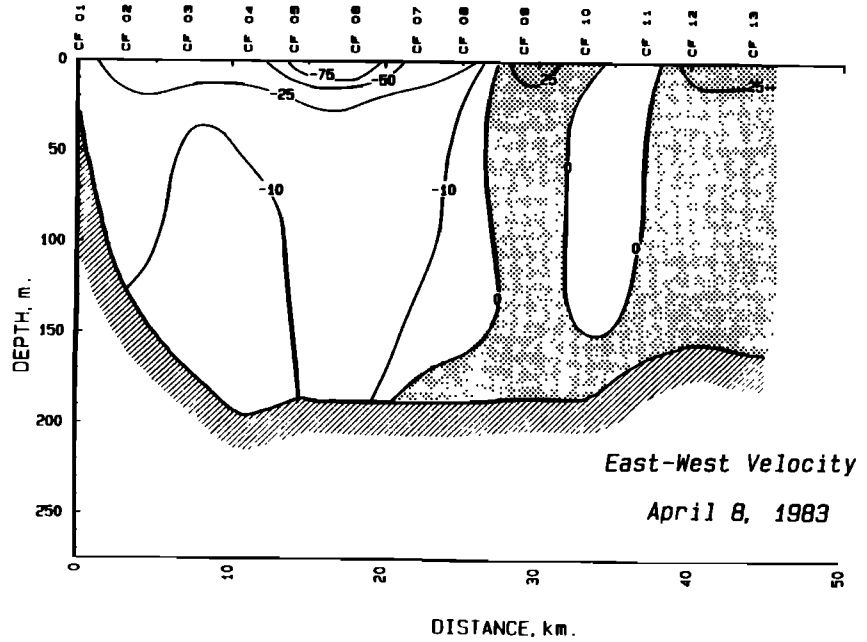

Fig. 7a

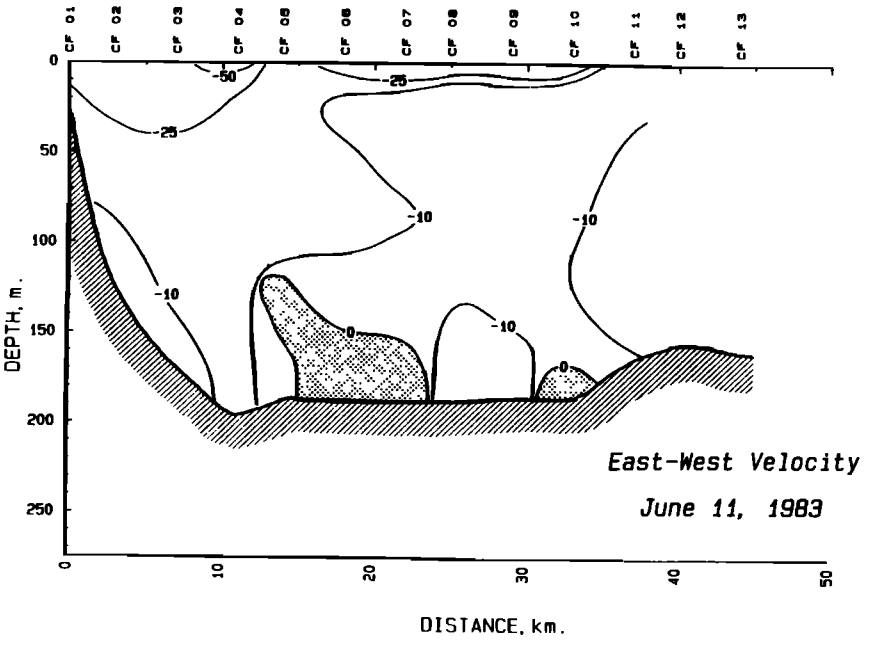

Fig. 7b

Fig. 7. East-west velocity component (centimeters per second) on the Cape Fairfield line determined by PCM. Positive (eastward) values are shaded. (*a*) April 1983; (*b*) June 1983; (*c*) September 8-9, 1983; (*d*) September 11, 1983; (*e*) October 1983; (*f*) May 1984; (*g*) June 1984; (*h*) August 1984; (*i*) October 1984.

although the velocities were generally small (25 cm s^{-1} or less). The offshore (southern) end of the section also contained eastward flow. In the June 1983 section, the *u* velocity was westward nearly everywhere with some small eastward flow found near the bottom between CF5 and CF7 and at CF10 (Figure 7*b*). The maximum velocities were only about -50 cm s^{-1}, and the core of the jet was centered at CF 4, 12 km offshore, 6 km closer to shore than in April. The current enclosed by the -25 cm s^{-1} contour was deeper (about 40 m) at CF3 than it was in April.

There were two velocity cross sections acquired in September 1983. The first indicated very large westward velocities, up to -180 cm s^{-1} in the core with the jet centered at CF7 about 23 km offshore (Figure 7*c*). The greatest velocities extended from CF4 to CF9 (12-30 km). Eastward flows were found offshore of CF9 and between 50 and 150 m.

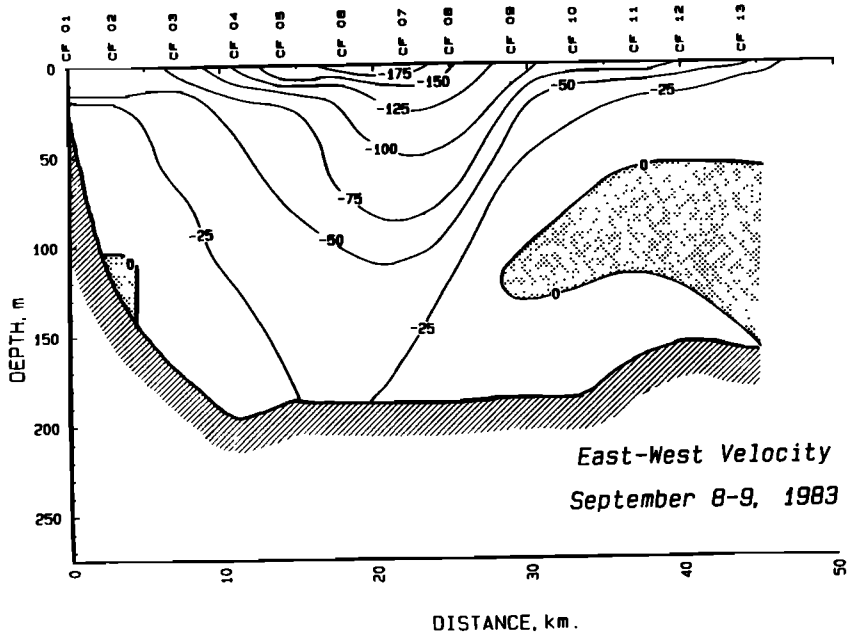

Fig. 7c

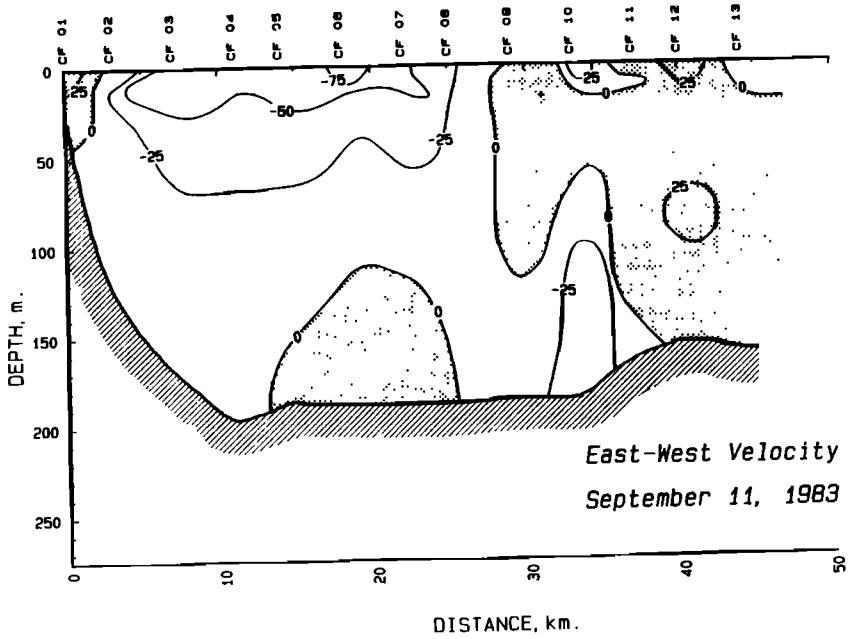

Fig. 7d

The second section in September 1983 (Figure 7*d*) was taken approximately 2 days later and had significantly smaller velocities than the first (Figure 7*c*). The maximum velocities were -80 cm s^{-1}, and the region included by the -25 cm s^{-1} contour extended from CF2 to CF8 and to 70-m depth. Eastward flow occurred offshore of CF9, and near bottom beneath the jet. In the October 1983 section (Figure 7*e*), the maximum velocity was over -75 cm s^{-1} at 4 km offshore, the closest approach of the maximum flow axis to the coast of any of the 1983 sections. Westward velocities were measured out to 35 km offshore, and strong (>75 cm s^{-1}) eastward flow was indicated at the offshore end of the section.

The 1984 PCM observations are, in general, similar to those from 1983. In May 1984 (Figure 7*f*), the westward jet was weak, with -25 cm s^{-1} at CF2 and -30 cm s^{-1} at CF5.

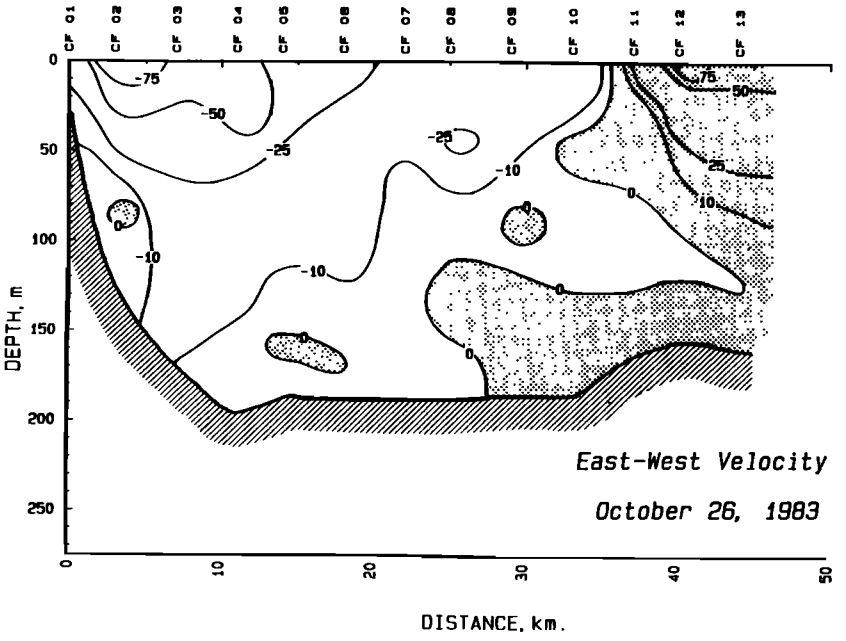

Fig. 7e

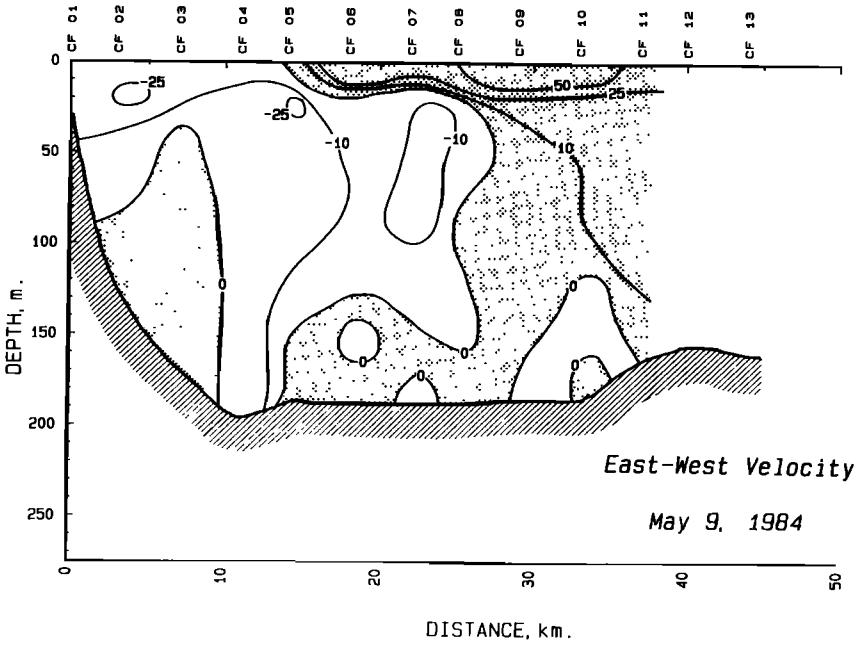

Fig. 7f

Eastward flow occurred offshore of CF8 and beneath the nearshore jet at CF2 and CF3. By June 1984 (Figure 7g), the jet had strengthened and widened, with the center of the jet between CF6 and CF7 (about 20 km offshore). There was eastward flow across the midshelf portion of the section (CF9). Westward flow was evident at CF10 through CF12, though there was eastward flow beyond CF12.

The August 1984 section (HX61) contains a departure from the normal flow distribution. In the August 1984 section (Figure 7h), the jet was centered at CF7 and CF8 (22-26 km). The flow was unusual in that eastward flow occurred over much of the shelf, with some of it inshore of the jet, between CF3 and CF5 (Figure 7h). Eastward flow also was observed in the subsurface, offshore part of the section, centered at CF11 and extending up to within 20 m of the surface. The velocity field at CF4 had little vertical shear. If this is an eddy, then it would probably be centered near CF6 and have anticyclonic rotation. The 0/100 dbar

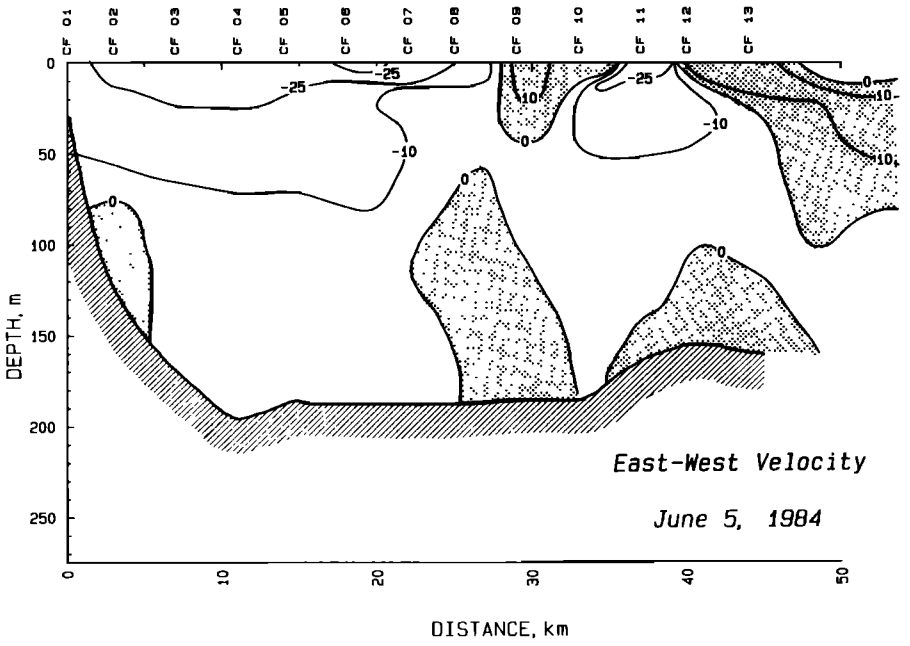

Fig. 7*g*

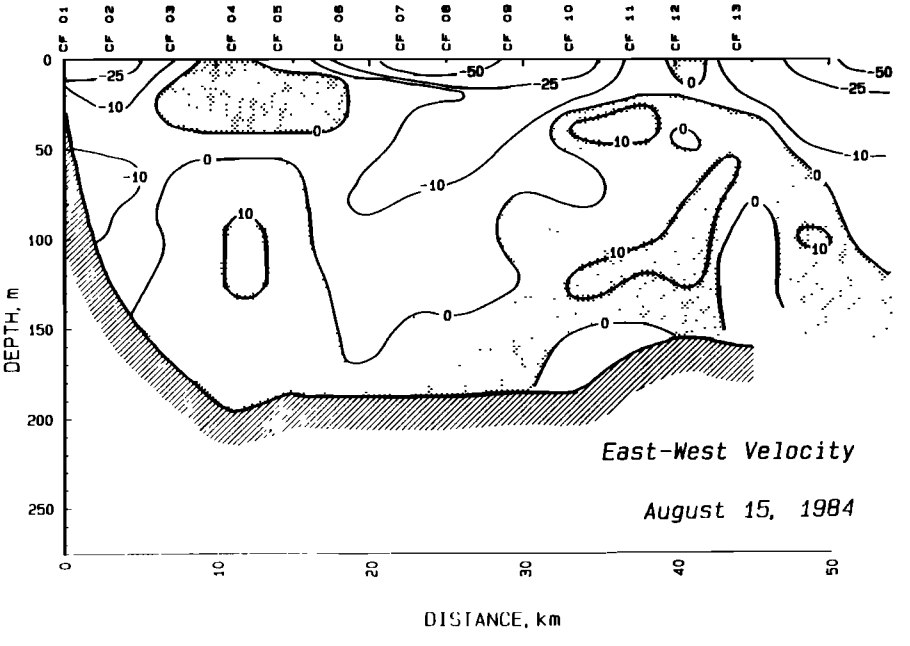

Fig. 7*h*

dynamic height topography supports the interpretation of an eddy or wavelike disturbance (Figure 6*g*). The August 1984 period has maximum mesoscale fluctuations in the dynamic height, and the PCM velocity cross section shows alongshore current reversals, characteristic of eddy-type circulation.

The October 1984 section (Figure 7*i*) had large westward flow (>100 cm s^{-1}), although it had to be discontinued due to high seas at CF7 (22 km offshore). The jet was centered at CF4, with speeds of over -100 cm s^{-1} and no eastward component was evident.

Current Meter Results

The PCM data provide a "snapshot" of the shelf circulation, temperature, and salinity, but continuous recording current meters are necessary to measure temporal variability. The mooring site was selected to be within the core of the coastal current for at least a portion of

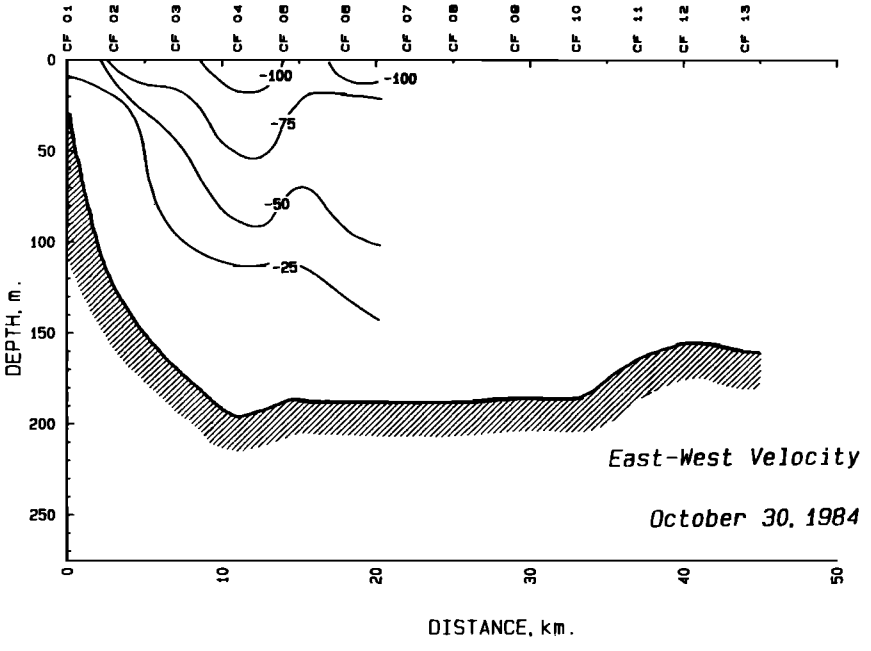

Fig. 7*i*

the year, and the position alongshore provided a regular topography upstream and downstream.

Monthly averaged time series. The monthly averaged currents from the moorings are presented as time depth contour plots (Figure 8, Tables 3 and 4). The averages for each of the current meters in Table 1 were calculated for calendar months. The east (u) current component near the surface strengthens to more than 50 cm s^{-1} westward in September 1983 and persists through February 1984, with the maximum westward value in January (Figure 8*a*, Table 3). The slope of the -20 and -10 cm s^{-1} contours indicates a delay of the maximum with depth from 2 to 4 months.

The v current component (onshore) was approximately an order of magnitude less than u (Figure 8*b*, Table 4). The greatest southward flow occurred near the surface in November 1983 (reaching -8 cm s^{-1}) between the two relative maxima in the u flow. At greater depths the flow was weaker, between -1.5 and 0.7 cm s^{-1}.

Temperature was greatest near the surface in August 1983 and least in March 1984 (Figure 8*c*). The vertical temperature gradient was smallest in March 1984, though a vertical density structure still existed. Vertical mixing did not result in a completely well mixed water column. The temperature maximum near the bottom (>7°C) occurred in November 1984, in accord with the seasonal variations described earlier [*Royer*, 1975].

Surface salinity was less than 28 ppt in August 1983 and increased to 31 ppt in January and February 1984 (Figure 8*d*). The depth of the 32-ppt isohaline was not as shallow in the latter part of the experiment as it was in the first months of the study.

The depth-averaged current from the mooring shows a maximum in the westward flow of more than 20 cm s^{-1} in January and February, following the time of the maximum transport. Increased downwelling favorable winds cause a narrowing and intensification of the jet without significantly altering the total transport [*Luick et al.*, 1987].

The monthly average data from the moorings were fit by the least squares method to the annual period (Table 5). Of interest here is the seasonal description, so any nonsinusoidal character of the annual cycle is discarded as part of the residual which will not be discussed. The amplitude of the u component of the annual cycle decreases with depth from more than 18 cm s^{-1} near the surface to less than 6 cm s^{-1} near the bottom. The amplitude of the v component has a maximum of 3.6 cm s^{-1} at the surface, is nearly zero at 70 m, and is about 1.6 cm s^{-1} near the bottom. The amplitude of the temperature variation decreases monotonically with depth from 3.8 at the surface to 1.4°C at the bottom. The salinity amplitude is a maximum near the surface and has a relative minimum at 50 m, increasing to 0.9 ppt at 70 m, and decreases to 0.5 ppt near the bottom. The phase of the deep time series is lagged relative to the surface for all the parameters (Figure 9). The largest phase differences occur for salinity and v velocity. Temperature has the smallest phase lag with depth, and also lags the other parameters by roughly 90° (3 months). The phase shift between temperature and salinity, particularly away from the surface, indicates that different processes are responsible for the variations. Near the surface, relatively warm and low salinity conditions occur nearly simultaneously, although the lowest salinities occur after the highest temperatures. This lag probably represents the delay in temperature for melting snow and ice in the discharge relative to the solar heating.

Spectrum analysis. The spectra from the 50 m (Figures 10*a* and 10*b*) and surface (Figures 10*c* and 10*d*) current meters show an increase in energy for most frequencies for the high-current period (September-November 1983) (Figures 10*b*and 10*d*) relative to the low-current period (April-June 1983) (Figures 10*a* and 10*c*). At 50 m, the energy increase appears to be primarily confined to the 0.15- to 0.4-cpd band, which could be the frequency band occupied by the wavelike disturbances if they propagate or advect with the current. At the surface, the energy increase

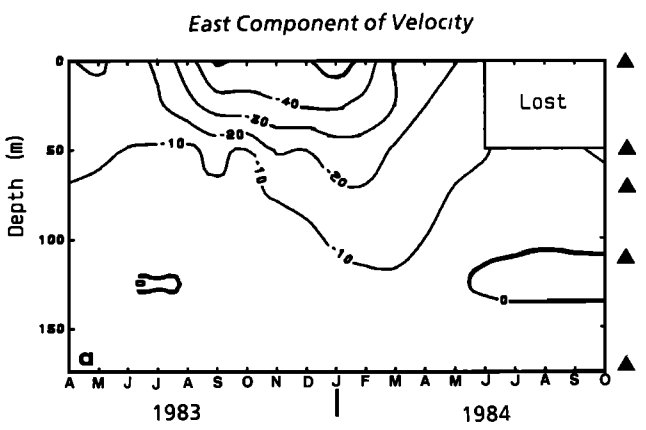

Fig. 8a

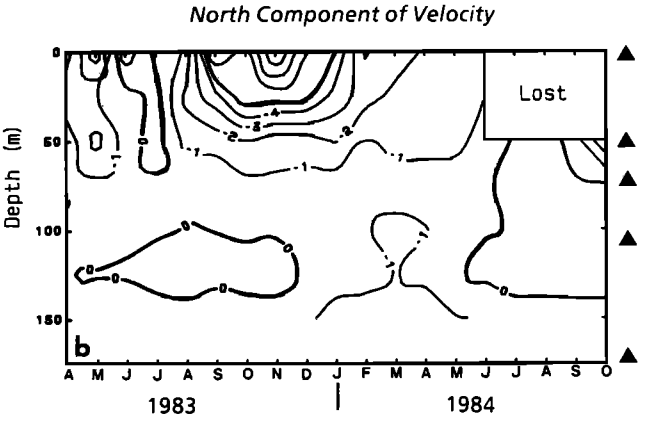

Fig. 8b

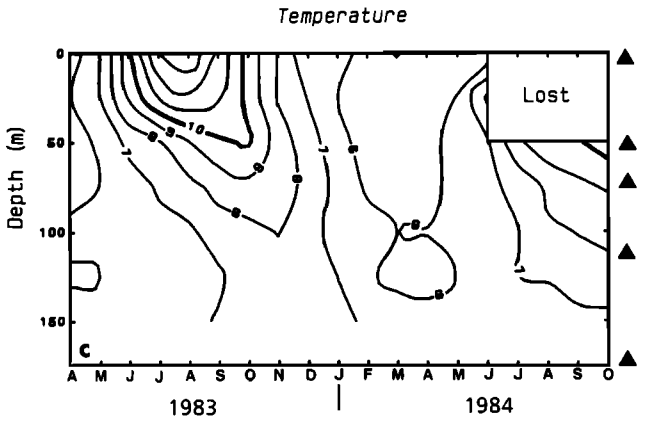

Fig. 8c

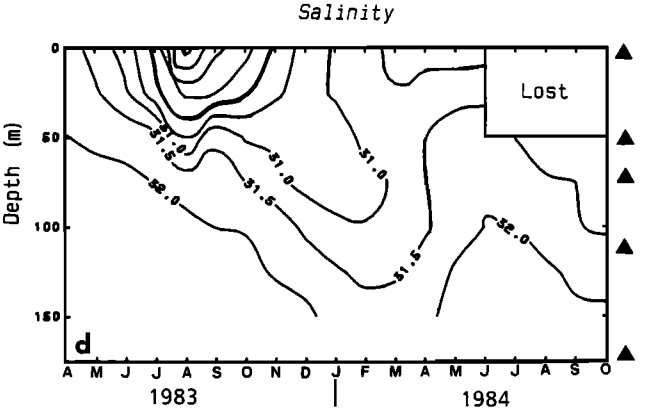

Fig. 8d

Fig. 8. Time versus depth contours of monthly averaged values from the current meters: (*a*) east-west velocity in centimeters per second, (*b*) north-south velocity in centimeters per second, (*c*) temperature in degrees Celsius, and (*d*) salinity in parts per thousand.

TABLE 3. East-West Velocity Component

	0 m		50 m		70 m		110 m		175 m	
Month	Mean	s.d.	Mean	s.d.	Mean	s.d.	Mean	s.d.	Mean	s.d.
1983										
April	-19.3	11.9	-13.2	6.8	-11.6	6.3	-6.9	6.1	-2.4	6.9
May	-22.4	12.4	-11.6	7.3	-9.0	6.2	-3.0	4.9	-0.1	5.4
June	-14.6	8.5	-9.7	5.3	-6.5	5.8	-0.5	3.8	0.7	4.3
July	-22.1	14.8	-8.9	7.1	-6.8	5.9	-1.1	3.6	0.5	4.6
Aug.	-35.6	21.8	-7.6	9.2	-7.0	7.2	-1.4	3.6	1.1	5.7
Sept.	-51.6	35.1	-13.9	12.9	-10.5	11.7	-6.0	9.2	-0.2	6.6
Oct.	-46.6	32.2	-9.9	13.4	-7.4	11.7	-1.9	10.0	-0.3	8.0
Nov.	-47.5	30.2	-21.2	11.9	-13.0	12.0	-2.4	11.6	0.2	7.6
Dec.	-48.8	20.8	-20.1	9.1	-14.5	7.7	-2.6	11.2	-0.3	6.3
1984										
Jan.	-54.8	20.2	-25.8	9.7	-20.8	8.1	-13.5	9.9	-3.4	9.9
Feb.	-47.3	20.8	-25.6	10.8	-22.2	9.0	-14.8	8.0	-6.1	9.1
March	-28.3	13.6	-18.8	8.3	-16.4	7.5	-11.4	7.9	-3.7	8.9
April	-20.3	10.9								
May			-13.3	6.2	-10.8	5.3	-3.9	7.5	-0.9	5.0
June			-11.3	6.4	-9.3	6.5	-3.2	6.8	1.2	5.2
July			-3.8	6.3	-1.6	7.8	2.9	6.7	0.6	5.3
Aug.			-2.9	9.0	-0.2	8.3	2.2	8.8	-0.1	4.5
Sept.			-8.8	12.3	-5.5	10.3	-0.3	6.8	0.3	6.7
Oct.			-12.9	15.0	-9.1	13.1	-3.1	4.7	0.1	7.1

TABLE 4. North-South Velocity Component

Month	0 m		50 m		70 m		110 m		175 m	
	Mean	s.d.	Mean	s.d.	Mean	s.d.	Mean	s.d.	Mean	s.d.
1983										
April	-0.4	8.5	-0.3	5.8	-0.6	4.6	-0.5	3.3	-0.6	4.9
May	-3.6	11.9	-2.3	6.1	-1.5	4.9	-0.5	3.9	-0.3	5.4
June	1.6	7.8	-0.5	5.0	-0.4	4.7	0.1	2.8	-0.5	3.9
July	-0.3	13.5	0.4	6.2	0.4	5.1	0.4	3.1	-0.3	4.8
Aug.	-1.1	24.6	-1.3	8.7	-1.1	5.6	-0.1	3.0	0.3	5.4
Sept.	-7.0	24.8	-1.4	9.4	0.5	8.3	0.2	7.1	-0.1	6.3
Oct.	-5.6	27.0	-2.0	12.5	-0.8	11.6	0.0	8.3	0.3	7.4
Nov.	-9.1	19.4	-1.5	9.6	-1.9	9.8	-0.3	8.4	-0.7	7.0
Dec.	-6.1	16.7	-1.5	7.9	0.0	6.8	1.2	7.1	-0.5	6.3
1984										
Jan.	-5	15.6	-2.1	8.6	-0.4	6.9	-1.1	7.1	-0.7	8.2
Feb.	-1.9	13.9	-1.0	8.1	-0.5	7.2	-1.6	7.2	-2.4	8.6
March	-2.6	10.4	-1.5	6.9	-0.3	6.2	-1.1	5.8	-1.5	6.5
April	-1.2	6.8								
May			-1.4	5.2	-0.7	4.8	-1.1	5.4	-0.9	4.7
June			-0.5	5.2	-0.3	5.6	0.2	5.3	-0.5	4.5
July			0.1	4.7	0.5	6.4	0.9	5.2	-0.1	4.4
Aug.			0.7	6.2	0.1	5.6	0.3	5.3	-0.8	4.5
Sept.			-0.7	10.6	0.6	8.3	0.5	4.3	0.3	5.9
Oct.			-2.9	14.4	-0.8	11.8	0.1	3.4	-0.1	6.3

is not as "banded" but is larger in magnitude at all frequencies during September-November.

The low-frequency part of the spectrum, 0.06 to 0.6 cpd, from the 50-m current meters was calculated for each month from April 1983 through March 1984. The results are shown as a contour plot of log spectral density against axes of months versus frequency (Figure 11). The plot shows an increase of energy over a wide range of frequency during the summer, from a June minimum to a September-October maximum. The 0.15- to 0.4-cpd band has the lowest energy at 50 m in June, which also has the smallest total variance. Conversely, the maximum low-frequency energy occurs in October 1983 at 50 m, at the time of the maximum transport, and not in November through January 1984 when the maximum currents occur at the mooring location (Figure 8*a*). Thus, the maximum low frequency energy appears to be closely related to the transport of the current. The spectrum at 0.5 cpd behaves differently, with a small relative minimum in October superimposed on the general trend of increase seen at the lower frequencies.

Empirical orthogonal function analysis. The relative importance of wind and freshwater forcing in producing seasonal changes in the currents was tested using empirical orthogonal function analysis. The analysis was performed on the correlation matrices constructed from the u component of the FNOC winds, the coastal freshwater discharge, and the time series from the current meters for each of the parameters. The correlation matrices were computed for the 1-year period April 1983 to March 1984 only. Only the first and second modes for each parameter are shown, with the total variance accounted for by the mode (Table 6).

The u component indicates large contributions to the first mode by the interior currents and the wind, and lesser contributions by the surface current meter and discharge. The signs of the weighting factors indicate that when the wind strengthens to the west, the current strengthens to the west as well. The second mode has major contributions from the discharge and the near-surface currents and small contributions by the near-bottom currents and the wind. The signs are such that an increase in the discharge is related to a westward increase in the near-surface current. This analysis shows that there is a distinct separation of the near-surface current from the interior currents.

The first mode of the v (onshore) velocity indicates some contribution at all depths is related to the wind, and the discharge is much smaller. The signs of the weights show that when the wind is westward, the flow is southward, probably because of the orientation of the coast downstream to the west of the mooring. The second mode shows a distributed relation of the currents and discharge. The signs of the weights indicate that when the discharge is large the flow is south (offshore) at the surface and north

TABLE 5. Results of Fit to Annual Period

Depth	East-West		North-South		Salinity		Temperature	
	Amplitude	Phase	Amplitude	Phase	Amplitude	Phase	Amplitude	Phase
2	18.1	42.4	3.6	36.2	1.39	-33.0	3.99	124.7
50	8.1	93.6	0.5	60.3	0.57	40.3	2.31	156.2
70	6.7	103.6	0.1	95.0	0.78	71.8	1.79	171.4
110	5.4	119.3	0.7	142.3	0.60	108.9	1.20	-174.0
175	2.5	124.0	0.8	130.6	0.41	109.7	0.71	-156.7

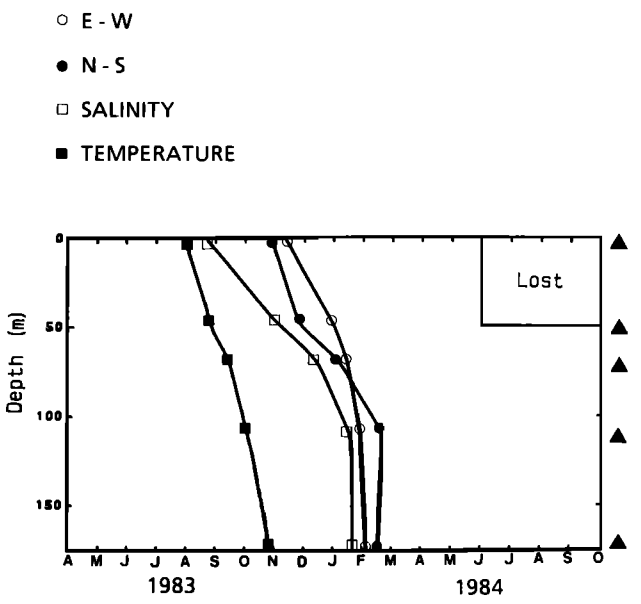

Fig. 9. Time of extremes in the seasonal cycle as determined by least squares fit to annual period.

(onshore) at the bottom. This suggests that an entrainment process is occurring. The wind makes no contribution to this mode.

The first mode for temperature has its major contributions from discharge, with much smaller effects from the wind. The signs indicate that when the discharge is high, the temperature is high. The second mode has a large contribution by the wind, and the temperature relation varies with depth, from positively related to the wind near the surface to negatively related near the bottom. Thus when the wind is westward, the temperature is cooler at the surface and relatively warmer near the bottom. The reversal of the contributions of wind and discharge to the temperature modes is in part related to the phase difference of temperature to the other parameters, which was about 3 months.

The first mode for salinity has large contributions from the wind and the interior currents, with the 50-m and near-surface currents giving smaller estimates. In the interior, when the wind is more westward, the salinity is below average, consistent with downwelling. At the surface, when the wind is more westward, the salinity increases. This could be a consequence of the coastal current being displaced shoreward of the mooring at CF3. The second mode for salinity is, as before, a discharge related mode, with no significant contribution by wind. The salinity is related to discharge only at the surface, 50 m, and 70 m, and the signs are such that when the discharge is above average, the salinity is below average, as might be expected on the basis of dilution. The dilution is limited to depths of less than 110 m.

The mode analyses indicate a strong relationship between the east-west wind and the flow in the current. When the wind intensifies, it affects the flow and salinity structure. The discharge has a major role in the secondary circulation, particularly indicated by the onshore-offshore flow. This secondary circulation is a one-cell circulation with offshore flow of warm, fresh water at the surface during high discharge periods, compensated for by onshore flow of water at depth. This circulation appears to dominate over the Ekman circulation on the monthly averaged time scale and little, if any, onshore flow during downwelling favorable conditions is indicated.

SUMMARY

This field study of the Alaska Coastal Current has revealed several new aspects of the flow. The seasonal maximum of the current shows that the westward velocity is much stronger than expected, being one of the most intense coastal currents yet reported. The observations confirm the westward coastal current with a mean flow of about 35 cm s^{-1} at the surface, decreasing with depth to near

TABLE 6. Eigen Analysis Results

	East-West		North-South		Temperature		Salinity	
	Mode 1	Mode 2	Mode 1	Mode 2	Mode 1	Mode 2	Mode 1	Mode 2
Eigenvalue	4.75	1.22	2.52	2.15	4.04	2.04	4.11	1.78
Variance, %	67.81	17.48	35.94	30.77	57.73	29.11	58.72	25.48
Eigenvectors								
Depth								
2 m	0.252	-0.669	-0.284	-0.512	-0.339	-0.432	0.210	0.647
50 m	0.441	-0.138	-0.387	-0.416	-0.483	-0.118	-0.284	0.574
70 m	0.457	0.022	-0.291	-0.261	-0.482	0.099	-0.443	0.266
110 m	0.410	0.173	-0.421	0.279	-0.424	0.337	-0.452	-0.026
175 m	0.403	0.255	-0.410	0.447	-0.335	0.472	-0.449	-0.066
E-W Wind	0.386	-0.249	-0.564	0.022	-0.115	-0.638	-0.438	0.036
Discharge	0.231	0.613	-0.147	0.468	-0.338	-0.214	-0.284	-0.419
Percent Variance Explained for Each Series								
Depth								
2 m	30.25	54.75	20.31	56.38	46.35	37.95	18.18	74.66
50 m	92.19	2.32	37.66	37.26	94.43	2.81	33.08	58.75
70 m	99.30	0.06	21.26	14.64	93.99	1.98	80.76	12.60
110 m	79.84	3.65	44.68	16.79	72.56	23.19	84.04	0.12
175 m	77.20	7.97	42.33	42.98	45.28	45.44	82.84	0.77
E-W Wind	70.58	7.57	79.89	0.10	5.31	83.07	78.96	0.23
Discharge	25.34	46.03	5.43	47.25	46.21	9.35	33.22	31.24

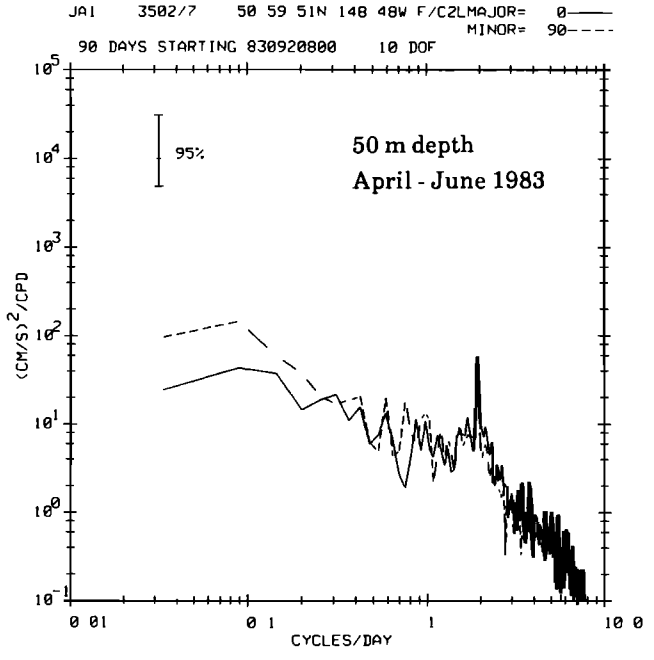

Fig. 10a

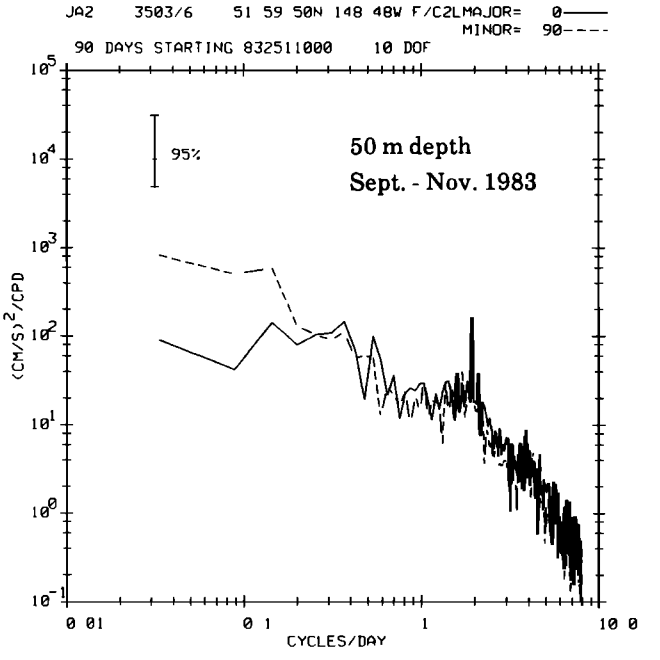

Fig. 10b

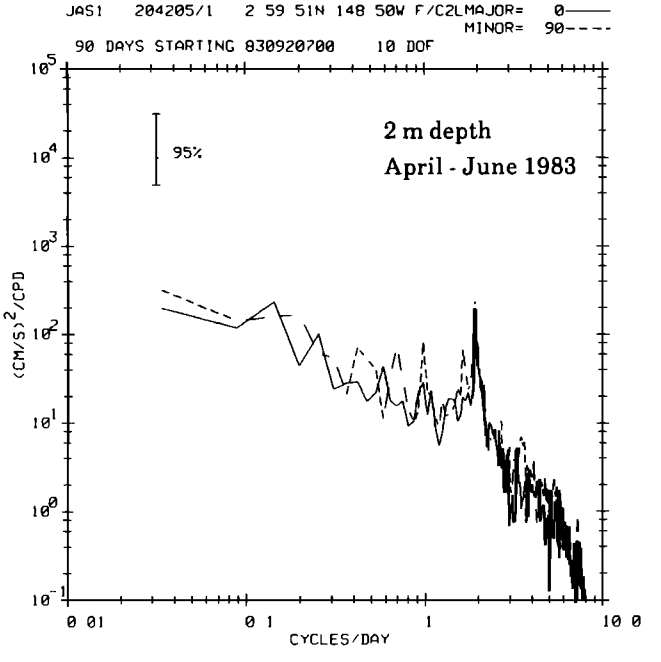

Fig. 10c

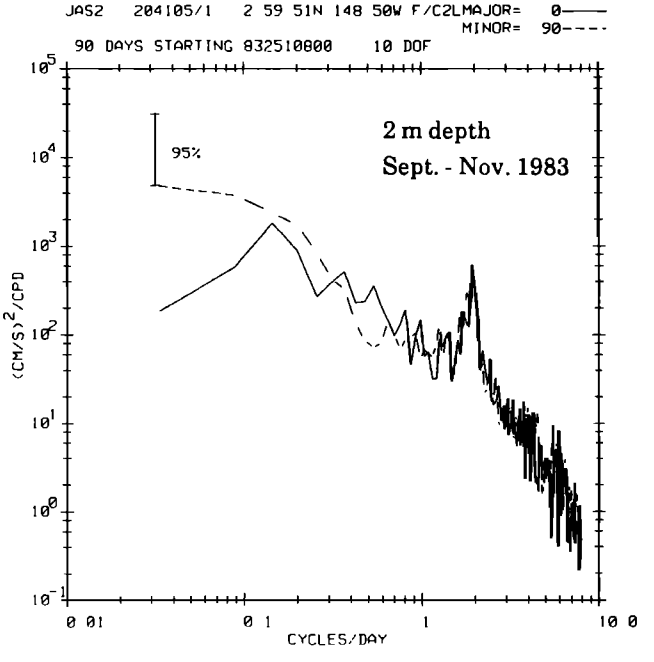

Fig. 10d

Fig. 10. Spectra calculated for 90-day sections of data at (*a*) 50-m depth, April-June 1983; (*b*) 50-m depth, September-November 1983; (*c*) 2-m depth, April-June 1983; and (*d*) 2-m depth, September-November 1983. The solid lines are north-south velocity; the dashed lines are east-west velocity.

zero. The annual variation of the westward flow decreases in amplitude with depth, and the phase is delayed by 3 months at 175 m. The amplitude of the annual cycle of the north-south flow is the largest near the surface and the bottom. The phase of the seasonal cycle is again delayed at deeper depths, but the maximum shift relative to the surface occurs at 110 m rather than at 175 m.

Empirical orthogonal function analysis shows that the first mode of the alongshore flow is nearly barotropic and is related to the east-west wind. The second mode is composed of the surface current and the runoff. The cross-shore flow analysis shows that the first mode is again nearly barotropic and principally related to the east-west wind, although the sign of the surface current contradicts a simple Ekman circulation. The second mode fluctuates with discharge and indicates that offshore flow at the

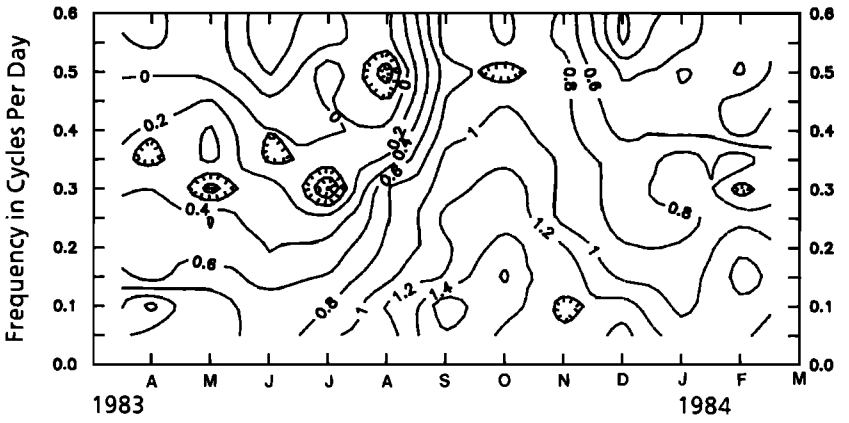

Fig. 11. Contours of log kinetic energy spectral density from 50-m depth. Axes are months of 1983 and 1984 versus frequency in cycles per day.

surface and onshore flow near the bottom are related to large values of discharge.

At the time of maximum transport of the current, the eddy energy level also increases. The dynamic topography indicates more complicated patterns during the high-transport season of the year than in the low-transport period. This is probably due to a baroclinic instability mechanism [*Mysak et al.*, 1981]. As such, it represents a mechanism through which much more rapid mixing of coastal water onto the shelf could occur, and shelf water can be brought into the coastal domain.

Acknowledgments. We would like to acknowledge the important contributions made by David Nebert and John Smithhisler in conducting the field program, designing and fabricating the moorings, and preparing and deploying the current meters. David Boisseau helped greatly in deploying the moorings. The captain, crew and shipboard technicians of the R/V *Alpha Helix* are thanked for their help in all of the field operations. This project was supported by NSF grants OCE 8208306 and OCE 8614549. Institute of Marine Science, University of Alaska Fairbanks, contribution 671.

REFERENCES

Düing, W., and D. R. Johnson, High resolution current profiling in the Straits of Florida, *Deep Sea Res.*, *19*, 259-274, 1972.

Favorite, F., Flow into the Bering Sea through Aleutian passes, in *Oceanography of the Bering Sea with Emphasis on Renewable Resources*, edited by D. W. Hood and E. J. Kelley, pp. 3-38, Institute of Marine Science, University of Alaska, Fairbanks, 1974.

Johnson, W. R., and T. C. Royer, A comparison of two current meters of a surface mooring, *Deep Sea Res.*, *33*, 1127-1138, 1986.

Luick, J. L., T. C. Royer, and W. R. Johnson, Coastal atmospheric forcing in the northern Gulf of Alaska, *J. Geophys. Res.*, *92*, 3841-3848, 1987.

Mork, M., Experiments with theoretical models of the Norwegian Coastal Current, in *The Norwegian Coastal Current*, vol. III, edited by R. Saetre and M. Mork, pp. 518-530, University of Bergen, Bergen, Norway, 1981.

Mysak, L. A., R. D. Muench, and J. D. Schumacher, Baroclinic instability in a downstream channel: Shelikov Strait, Alaska, *J. Phys. Oceanogr.*, *11*, 950-969, 1981.

Pattullo, J., W. Munk, R. Revelle, and E. Strong, The seasonal oscillation in sea level, *J. Mar. Res.*, *14*, 88-155, 1955.

Reid, J. L., and A. W. Mantyla, The effect of geostrophic flow upon coastal sea elevations in the northern North Pacific Ocean, *J. Geophys. Res.*, *81*, 3100-3110, 1976.

Royer, T. C., Seasonal variations of waters in the northern Gulf of Alaska, *Deep Sea Res.*, *22*, 403-416, 1975.

Royer, T. C., On the effect of precipitation and runoff on coastal circulation in the Gulf of Alaska, *J. Phys. Oceanogr.*, *9*, 555-563, 1979.

Royer, T. C., Baroclinic transport in the Gulf of Alaska, II, A fresh water driven coastal current, *J. Mar. Res.*, *39*, 251-266, 1981.

Royer, T. C., Coastal fresh water discharge in the northeast Pacific, *J. Geophys. Res.*, *87*, 2017-2021, 1982.

Schumacher, J. D., and R. Reed, Coastal flow in the northwest Gulf of Alaska: The Kenai Current, *J. Geophys. Res.*, *85*, 6680-6688, 1980.

Xiong, Q., and T. C. Royer, Coastal temperature and salinity in the northern Gulf of Alaska, 1970-1983, *J. Geophys. Res.*, *89*, 8061-8068, 1984.

W. R. Johnson, J. L. Luick, and T. C. Royer, Institute of Marine Science, University of Alaska Fairbanks, Fairbanks, AK 99775.

(Received December 28, 1987;
accepted February 9, 1988.)